NASA TN D-1497

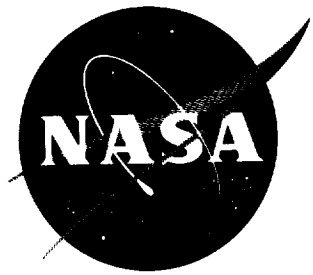

TECHNICAL NOTE

D-1497

STATIC STABILITY INVESTIGATION OF PROPOSED PROJECT FIRE SPACE-VEHICLE AND REENTRY-PACKAGE CONFIGURATIONS AT MACH NUMBERS FROM 1.47 TO 4.63

By Dennis E. Fuller and C. Donald Babb

Langley Research Center
Langley Station, Hampton, Va.

NATIONAL AERONAUTICS AND SPACE ADMINISTRATION
WASHINGTON
November 1962

NATIONAL AERONAUTICS AND SPACE ADMINISTRATION

TECHNICAL NOTE D-1497

STATIC STABILITY INVESTIGATION OF PROPOSED PROJECT FIRE SPACE-VEHICLE AND REENTRY-PACKAGE CONFIGURATIONS AT MACH NUMBERS FROM 1.47 TO 4.63

By Dennis E. Fuller and C. Donald Babb

SUMMARY

Tests were conducted in the Langley Unitary Plan wind tunnel on proposed space-vehicle and reentry-package model configurations for Project Fire. Five different second-stage velocity-reentry-package combinations were investigated as part of the two-stage space-vehicle configuration. Only one reentry-package configuration was tested. Tests were performed through an angle-of-attack range from about -7° to 18°, and a Mach number range from 1.47 to 4.63. The Reynolds number for these tests was held constant at 3.0×10^{6} per foot.

The results indicate that the variations in second stages have no significant effect on normal-force coefficients and only slight effects on the pitching-moment characteristics of the space-vehicle configurations tested. There are no large effects of Mach number, in the test Mach number range, on the normal-force or pitching-moment coefficients of the reentry-package configuration.

INTRODUCTION

The national space program, up to the present time, has concerned itself with the safe return of both instrumented and manned spacecraft from earth orbit, that is, reentry velocities of the order of 25,000 feet per second. Projected plans for the return of lunar or planetary probes, however, mean that returning spacecraft may reenter the earth's atmosphere at velocities of 36,000 to 45,000 feet per second. Although the heating rates during reentry have been fairly predictable for earth orbiting vehicles, the increased velocity of other types of spacecraft leads to less predictable heating rates, primarily due to radiative heating. In order to minimize the hazard of returning such spacecraft, Project Fire has been formulated at the Langley Research Center with the task of measuring total and radiative heat transfer and providing important data relating to materials behavior and radio-signal attenuation at reentry speeds in excess of those at which an earth orbiting vehicle would reenter.

As a part of the project, it is planned to mount a reentry package (spacecraft) on an Antares II (X-259) rocket (velocity package) which in turn will be launched on a ballistic trajectory by an Atlas D first-stage launch vehicle. The Antares rocket will then project the reentry package earthward at the required reentry velocities. The design of the velocity-reentry-package combination has not at present been finalized, and five possible shapes are currently proposed.

As a part of such a program, it is highly desirable to determine the static stability characteristics of the space-vehicle and reentry-package configurations in order that they may be stabilized if necessary to allow for suitable controllability. In addition, when rockets are staged, it is desirable to determine the aerodynamic loads in order that mating of such stages may be constructed with sufficient strength to avoid failure.

This paper contains axial-force and static longitudinal stability characteristics of a 0.03125-scale space-vehicle configuration composed of the Atlas D launch vehicle with five different proposed velocity-reentry-package shapes. These forces and moments were obtained on the overall space-vehicle configurations and on the velocity-reentry-package combinations alone (although attached to the first-stage launch vehicle). In addition, results are presented on a 0.316-scale model of a proposed reentry-package configuration. The tests were performed at Mach numbers from 1.47 to 4.63, at angles of attack from about -7° to 18°, and at a constant Reynolds number per foot of 3.0×10^{6}.

SYMBOLS

The aerodynamic force and moment data are referred to the body axes (fig. 1) with the origins located at the respective moment-center locations for each test configuration (fig. 2).

A reference area (space-vehicle configuration, 0.076699 sq ft; velocity-reentry-package combination, 0.076699 sq ft; reentry-package configuration, 0.349067 sq ft)

C_A axial-force coefficient, Axial force/qA

$C_{A,c}$ chamber-axial-force coefficient, Chamber axial force/qA

C_m pitching-moment coefficient, Pitching moment/qAd

C_N normal-force coefficient, Normal force/qA

d reference diameter (space-vehicle configuration, 3.750 in.; velocity-reentry-package combination, 3.750 in.; reentry-package configuration, 8.000 in.)

M free-stream Mach number

p_t free-stream stagnation pressure, lb/sq in. abs

q free-stream dynamic pressure, lb/sq ft

R_e Reynolds number, per foot

T_t stagnation temperature, $^{\circ}F$

α angle of attack of model center line, deg

DESCRIPTION OF APPARATUS

Tunnel

Tests were conducted in both the low and the high Mach number test sections of the Langley Unitary Plan wind tunnel which is a variable-pressure continuous-flow tunnel. The test sections are approximately 4 feet square and 7 feet long. The nozzles leading to the test sections are of the asymmetric sliding-block type, which permit a continuous variation in test-section Mach number from about 1.4 to 2.9 in the low Mach number test section, and from about 2.3 to 4.7 in the high Mach number test section.

Models

Drawings of the models tested are shown in figure 2. Typical photographs of models in the tunnel test section are presented as figure 3. The space-vehicle configurations consist of an Atlas D launch vehicle representing the first stage and five proposed velocity-reentry-package combinations representing the second stage. A gap of 0.040 inch separated the first- and second-stage model components and all data presented herein for the second-stage combinations are taken in the near proximity of the first stage. Hereinafter, each second-stage shape will be referred to by the number shown in figure 2. The aft, mating diameter of second-stage numbers 1, 2, 4, and 5 is the same as that for the fore, mating diameter of the first stage; however, the aft, mating diameter of second-stage number 3 was 0.157 inch larger than that for the other second stages, thus necessitating an adapter ring to be used on the first stage.

The reentry-package configuration (fig. 2(b)) is a blunt-nosed body with a 33° conical afterbody and a fineness ratio of about 0.73. The aft end of this configuration was modified to allow balance and sting attachment. (See fig. 3(b).)

It should be emphasized that the moment centers used in the data presentation for the space vehicle and second-stage velocity-reentry-package combinations do not represent true center-of-gravity locations. The moment center for the reentry-package model, however, is indicative of the actual center-of-gravity location.

PROCEDURE

Tests were performed at the following conditions:

M	T_t, °F	p_t, lb/sq in. abs	R_e, per foot
1.47	125	10.87	3.0×10^6
1.60	125	11.23	3.0
1.90	125	12.50	3.0
2.70	150	19.61	3.0
3.40	150	28.48	3.0
4.63	175	55.10	3.0

The dewpoint, measured at stagnation pressure, was maintained below -30° F to assure negligible condensation effects. The angle of attack was varied from approximately -7° to 18°, and the sideslip angle was maintained near 0°. All tests were conducted with natural boundary-layer transition.

The aerodynamic forces and moments of both the space-vehicle and reentry-package configurations were measured by means of internally mounted, strain-gage balances, which were, in turn, rigidly fastened to a sting support and thence to the tunnel support system. An internal strain-gage balance was also used to determine the forces and moments of the second-stage velocity-reentry-package combination, and this balance was securely fastened to a sting that was rigidly mounted to the first stage of the space-vehicle configuration.

Balance chamber pressure was measured by means of a single, static orifice located in the balance cavity of each model or part of a model.

CORRECTIONS AND ACCURACY

Angles of attack have been corrected for both tunnel flow angularity and deflection of sting and balance due to aerodynamic loads.

The axial-force coefficients presented are gross values and have not been adjusted to correspond to free-stream static pressure acting over the base. Chamber-axial-force coefficients, however, were determined for the space-vehicle configuration and the second-stage portion of the space-vehicle configuration and are presented in figure 4..

Based upon calibrations and repeatability of data, it is estimated that the various measured quantities are accurate within the following limits:

M = 1.47 to 3.40 . . . . . ±0.015
M = 4.63 . . . . . ±0.050

α, deg	±0.10
$C_{A,C}$	±0.0039
Space-vehicle configuration:	
C_A	±0.0025
C_m	±0.006
C_N	±0.006
Velocity-reentry-package combination:	
C_A	±0.006
C_M	±0.001
C_N	±0.003
Reentry-package configuration:	
C_A	±0.006
C_m	±0.0015
C_N	±0.005

PRESENTATION OF RESULTS

The results are presented in the following figures:

	Figure
Aerodynamic characteristics in pitch of the second-stage velocity-reentry-package combination in the near proximity of the first-stage launch vehicle	5
Aerodynamic characteristics in pitch of the space-vehicle configuration	6
Aerodynamic characteristics in pitch of the reentry-package configuration	7

SUMMARY OF RESULTS

Second-stage number 1 has the lowest normal-force slope and is the most stable of the five second-stage velocity-reentry-package configurations tested, throughout the test Mach number range. It also has the largest uncorrected axial-force coefficients probably because of the blunt nose and the "ring" encircling the second-stage casing. The greatest normal-force slope and the least stability are exhibited by second-stage number 3, whereas second-stage number 5, which has the smaller nose angle, produces the least uncorrected axial force.

The results for the complete space-vehicle configuration (fig. 6) indicate that none of the second stages have any significant effect on the normal-force coefficients, although slight changes in pitching moment are apparent and follow

the same trends for the complete space-vehicle configuration as those exhibited for the second stage alone.

There are no large effects of Mach number, in the test Mach number range, on the normal-force or pitching-moment coefficients of the reentry-package configuration, although there are abrupt discontinuities in the normal-force curves at negative angles of attack for Mach numbers of 1.60 and 1.90. (See fig. 7.) It is believed that these discontinuities are caused by asymmetric model conditions triggering separation of the boundary layer and probably will not be encountered under flight conditions. The axial force is lowest at $M = 1.47$ and peaks at a Mach number of 1.90 where essentially the same values are obtained up to $M = 4.63$. This trend in the variation of axial force with Mach number has been noted for other similar configurations such as those of reference 1.

Langley Research Center,
National Aeronautics and Space Administration,
Langley Station, Hampton, Va., August 6, 1962.

REFERENCE

1. Turner, Kenneth L., and Shaw, David S.: Wind-Tunnel Investigation at Mach Numbers From 1.60 to 4.50 of the Static-Stability Characteristics of Two Nonlifting Vehicles Suitable for Reentry. NASA MEMO 3-2-59L, 1959.

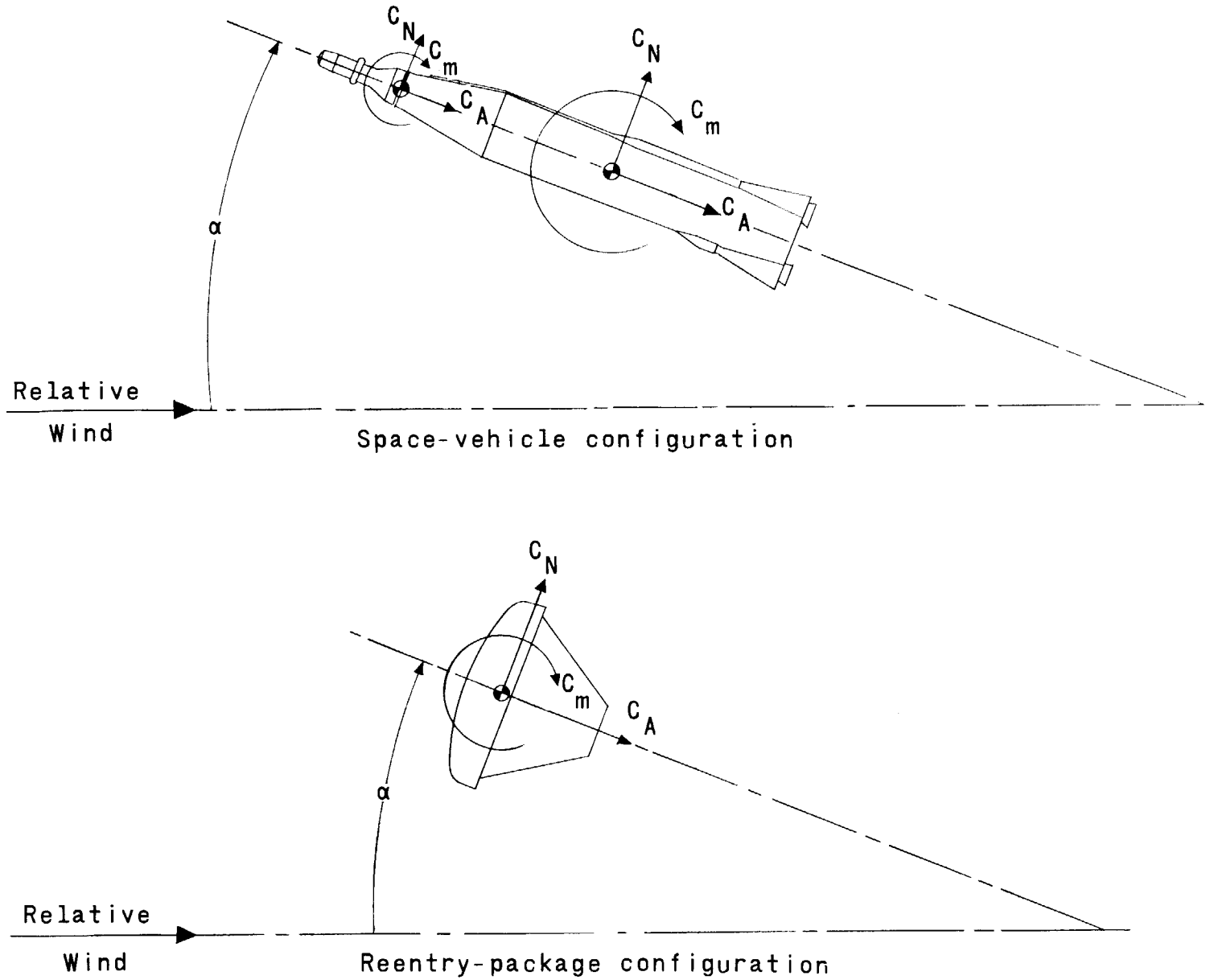

Figure 1.- Axis system. Arrows denote positive direction of forces and moments.

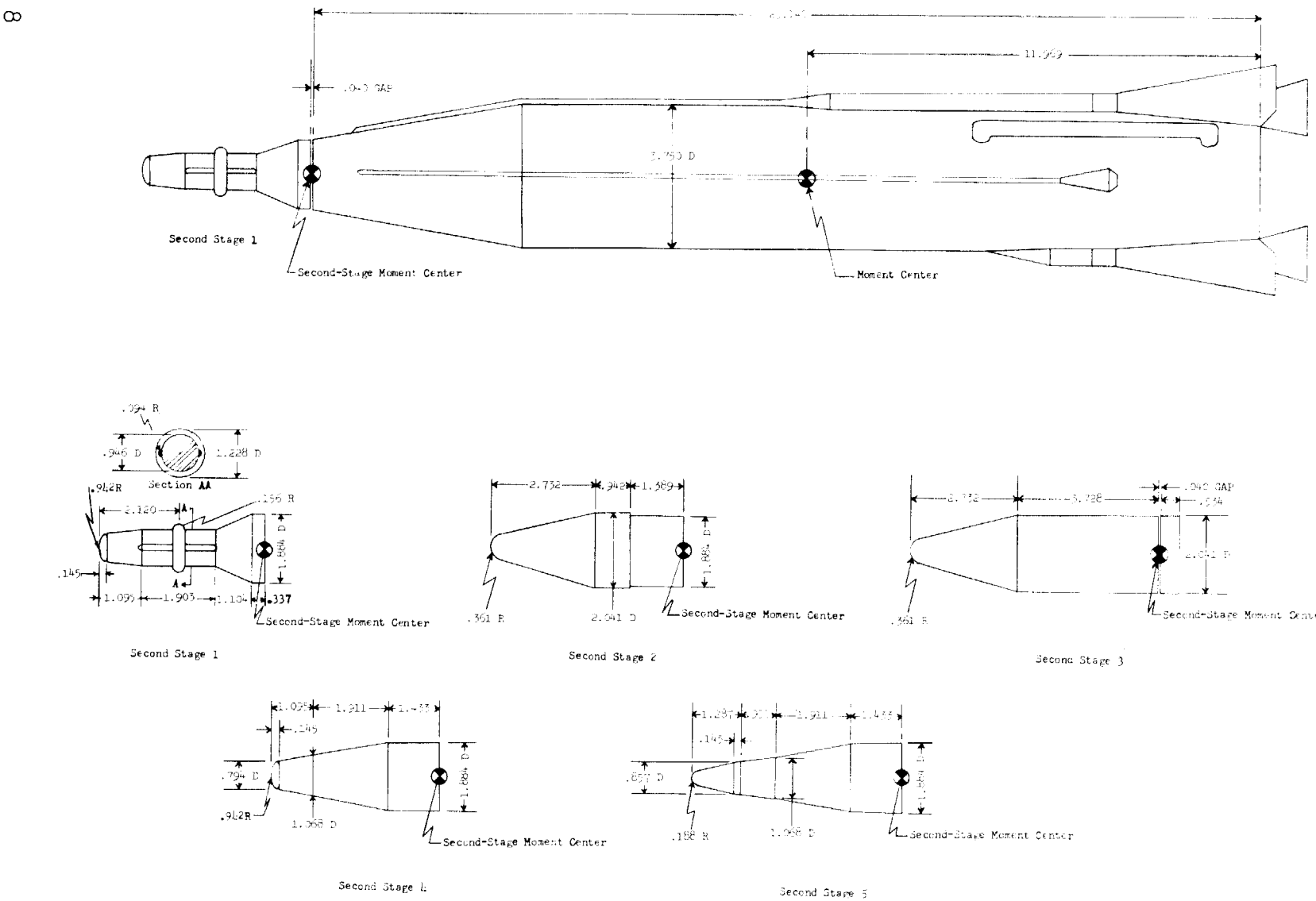

(a) Space-vehicle configuration.

Figure 2.- Dimensional details of test configurations. All dimensions in inches.

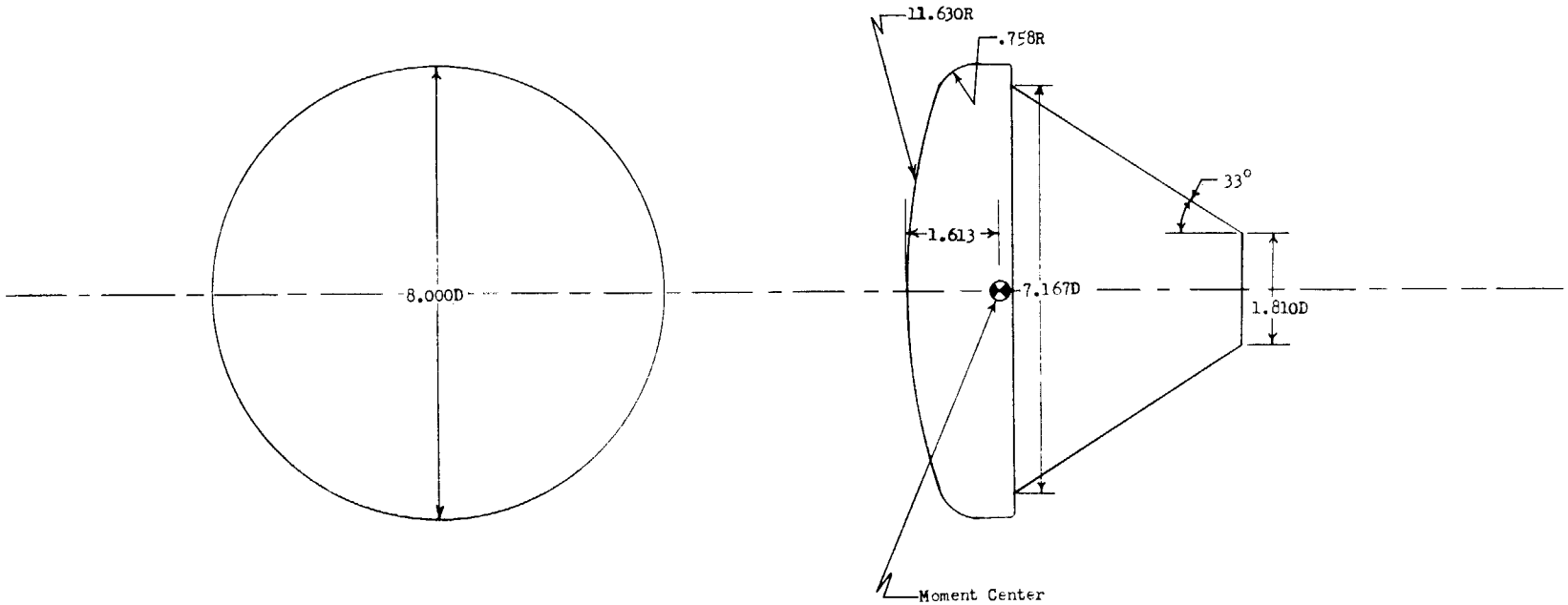

(b) Reentry-package configuration.

Figure 2.- Concluded.

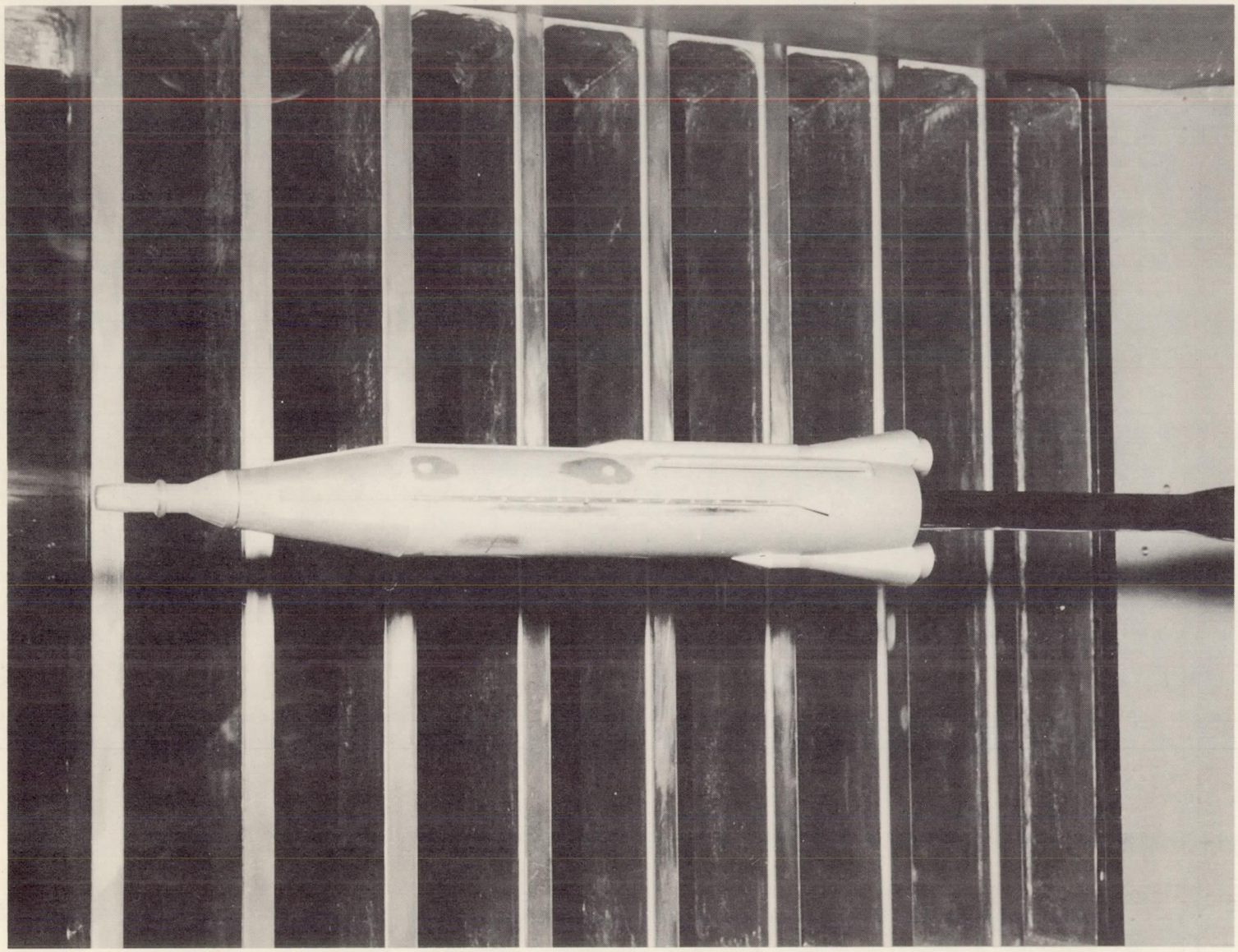

(a) Space-vehicle configuration. L-62-3475

Figure 3.- Typical model photographs.

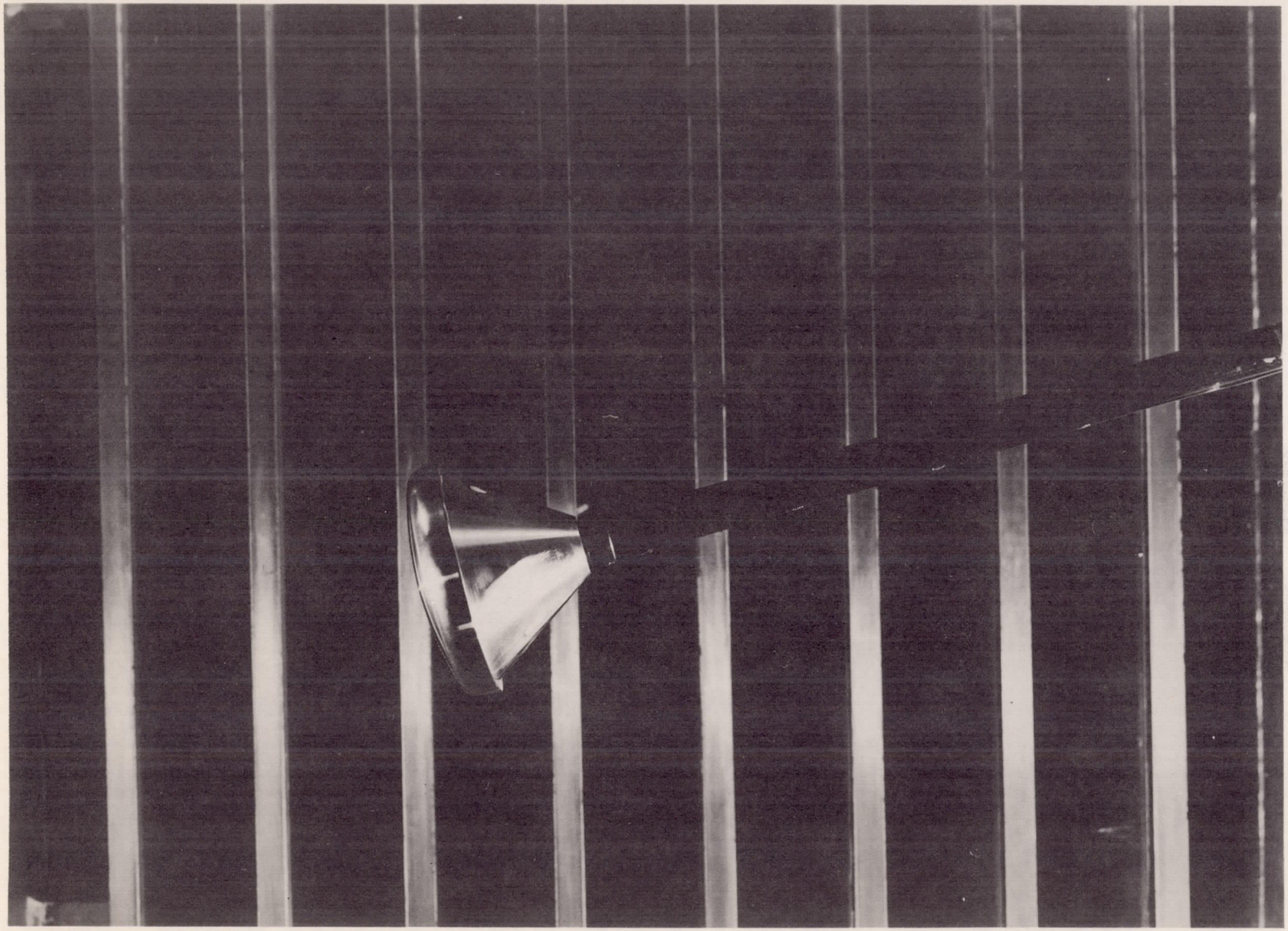

(b) Reentry-package configuration. L-62-3647

Figure 3.- Concluded.

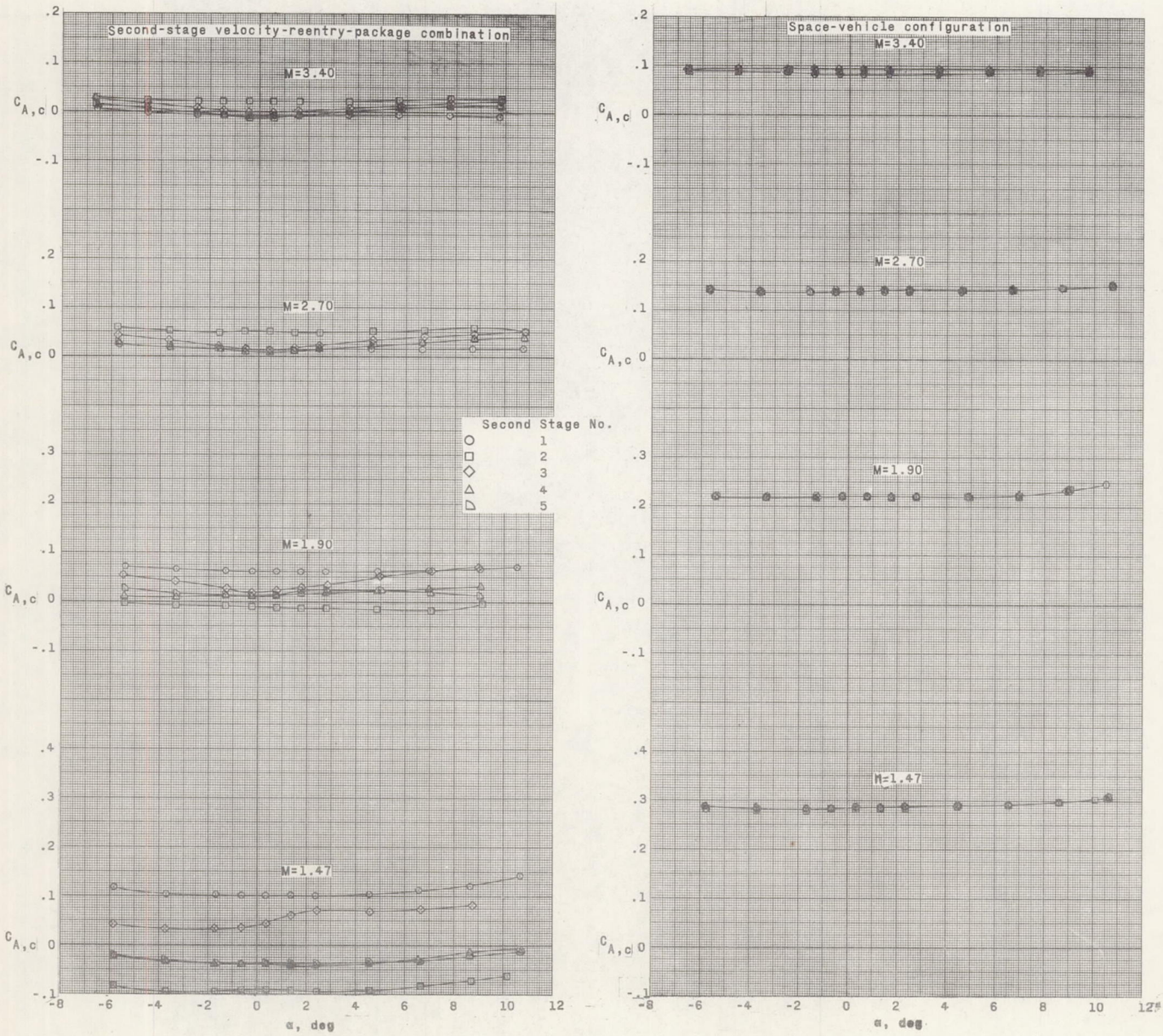

Figure 4.- Variation of chamber axial-force coefficient with angle of attack.

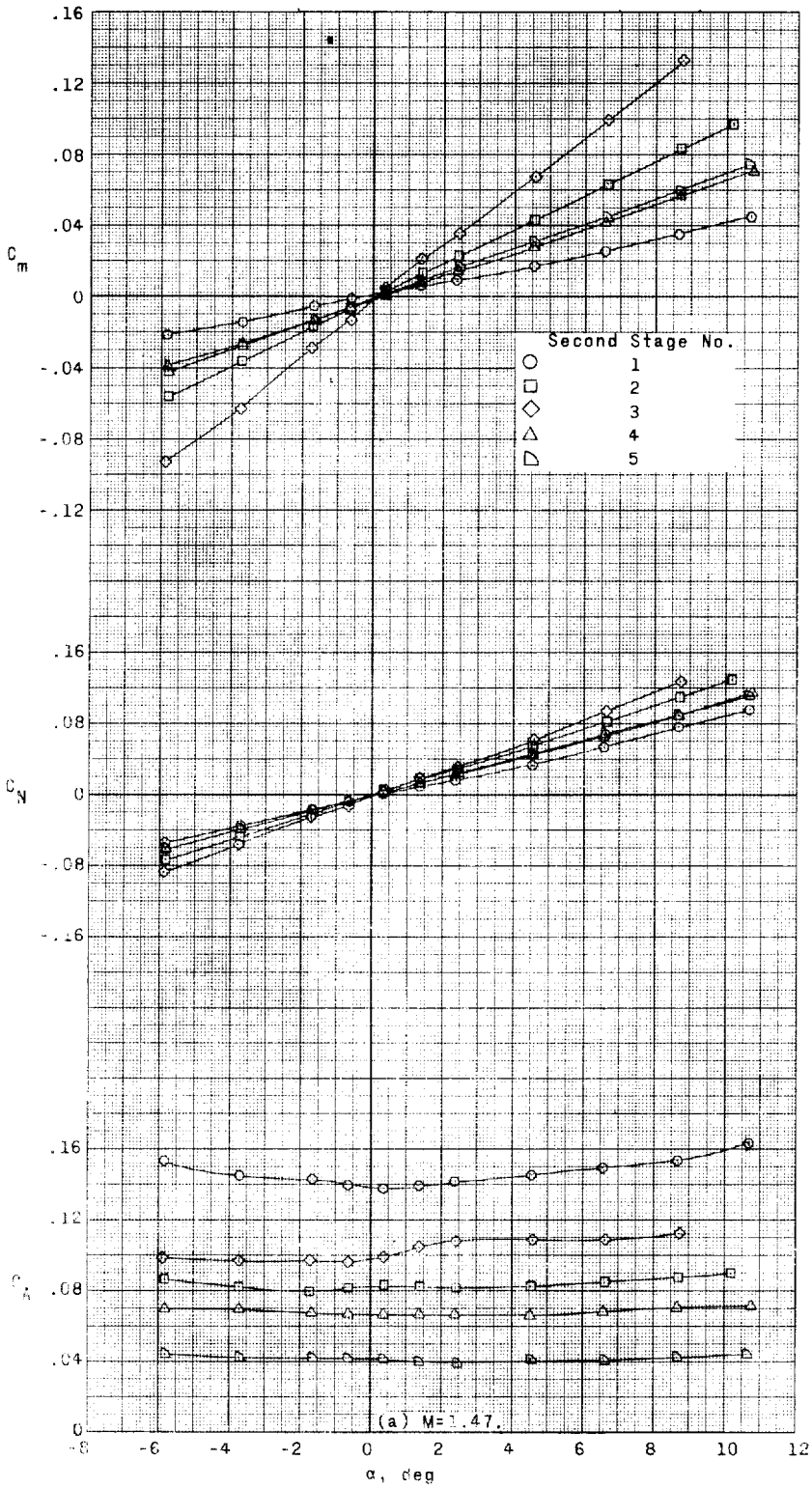

Figure 5.- Aerodynamic characteristics in pitch of the second-stage velocity-reentry-package combination in the near proximity of the first stage.

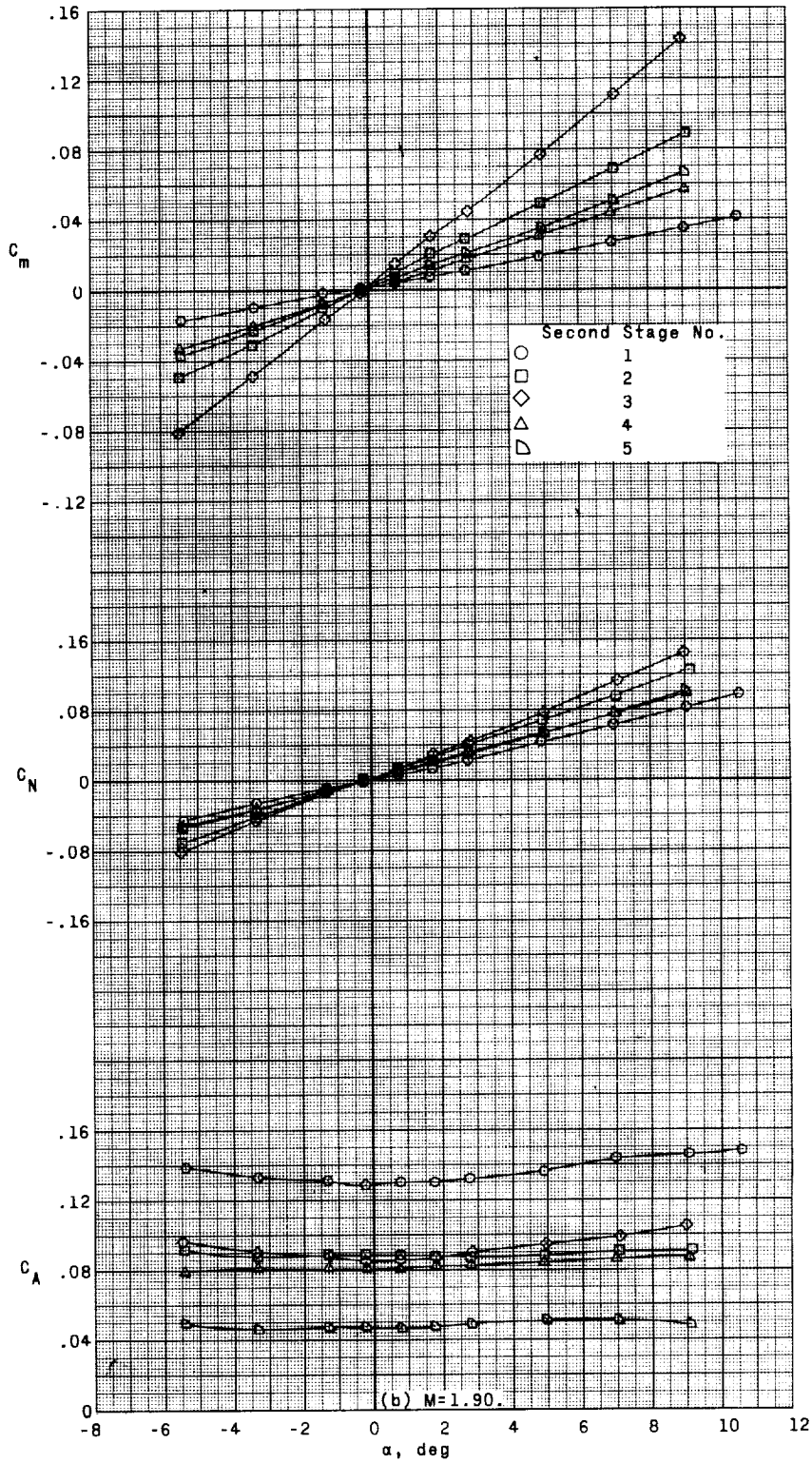

Figure 5.- Continued.

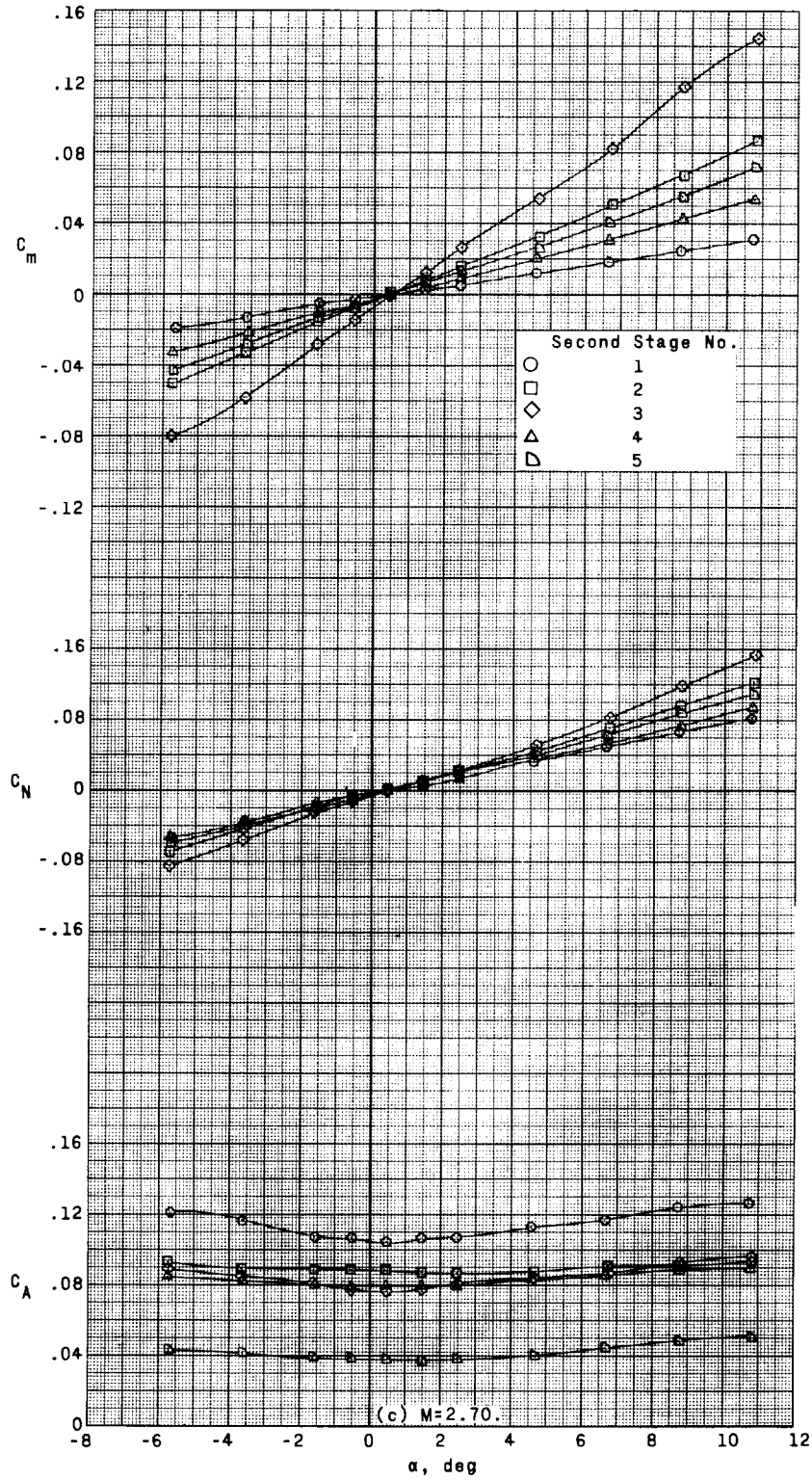

Figure 5.- Continued.

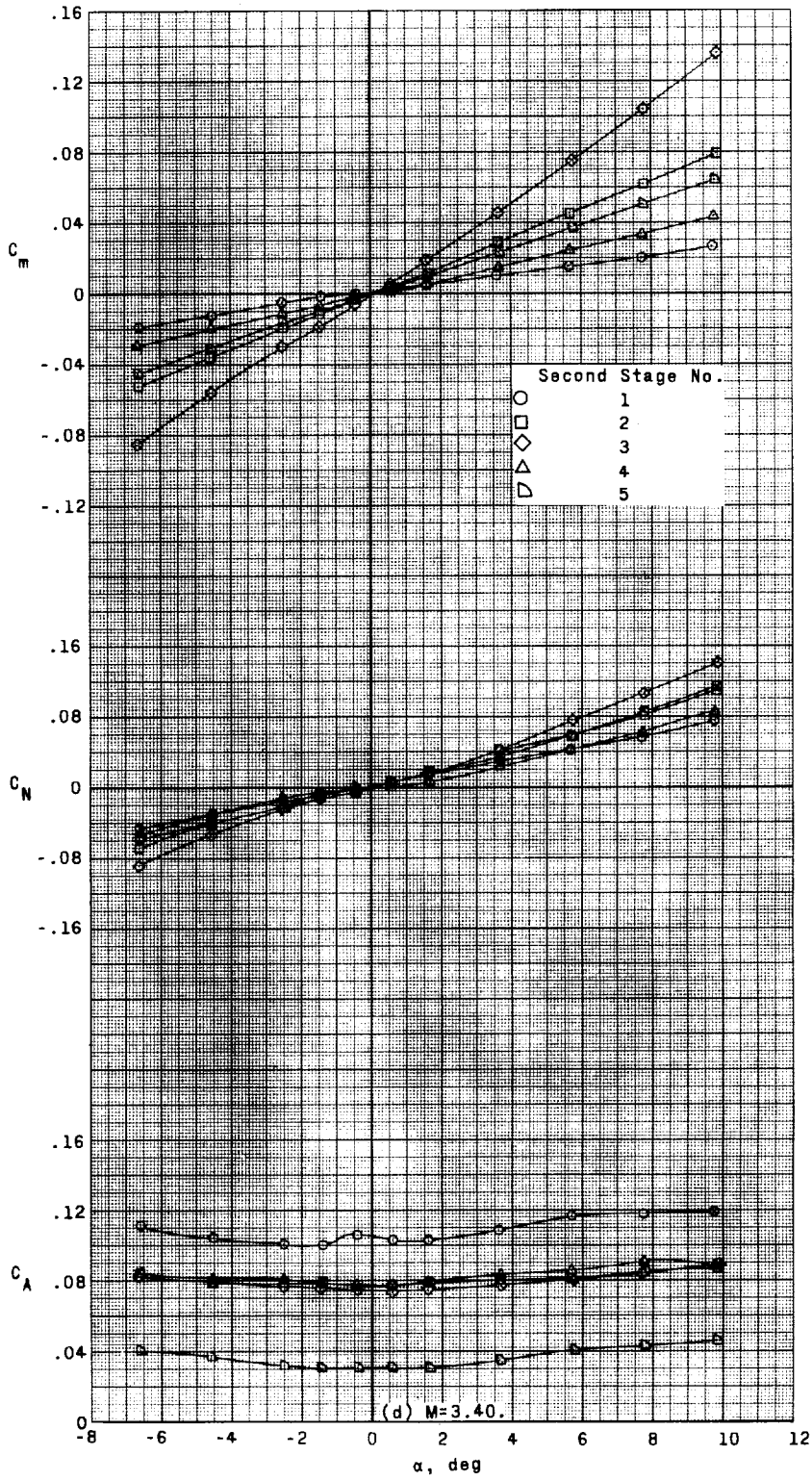

Figure 5.- Concluded.

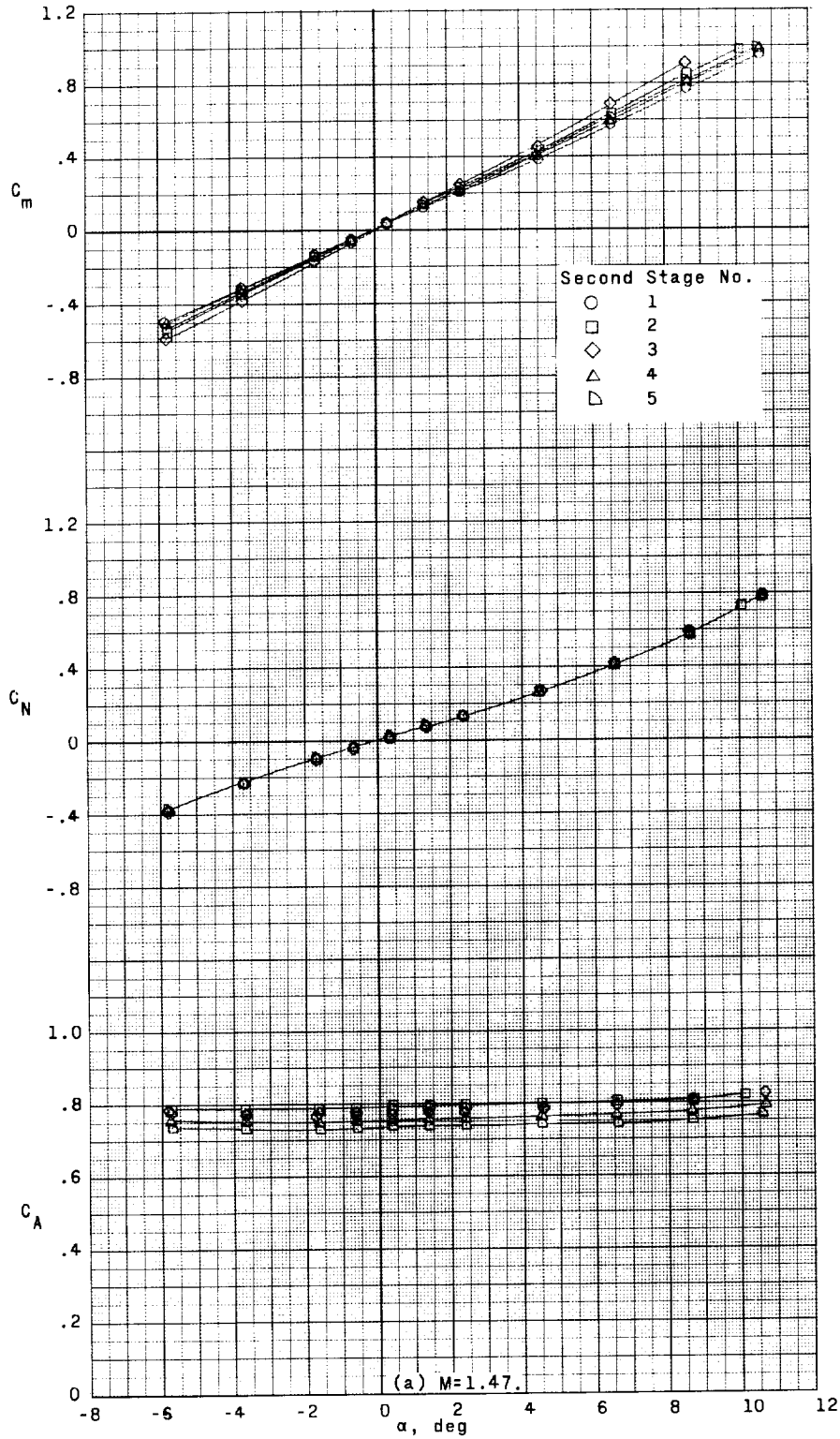

Figure 6.- Aerodynamic characteristics in pitch of the space-vehicle configuration.

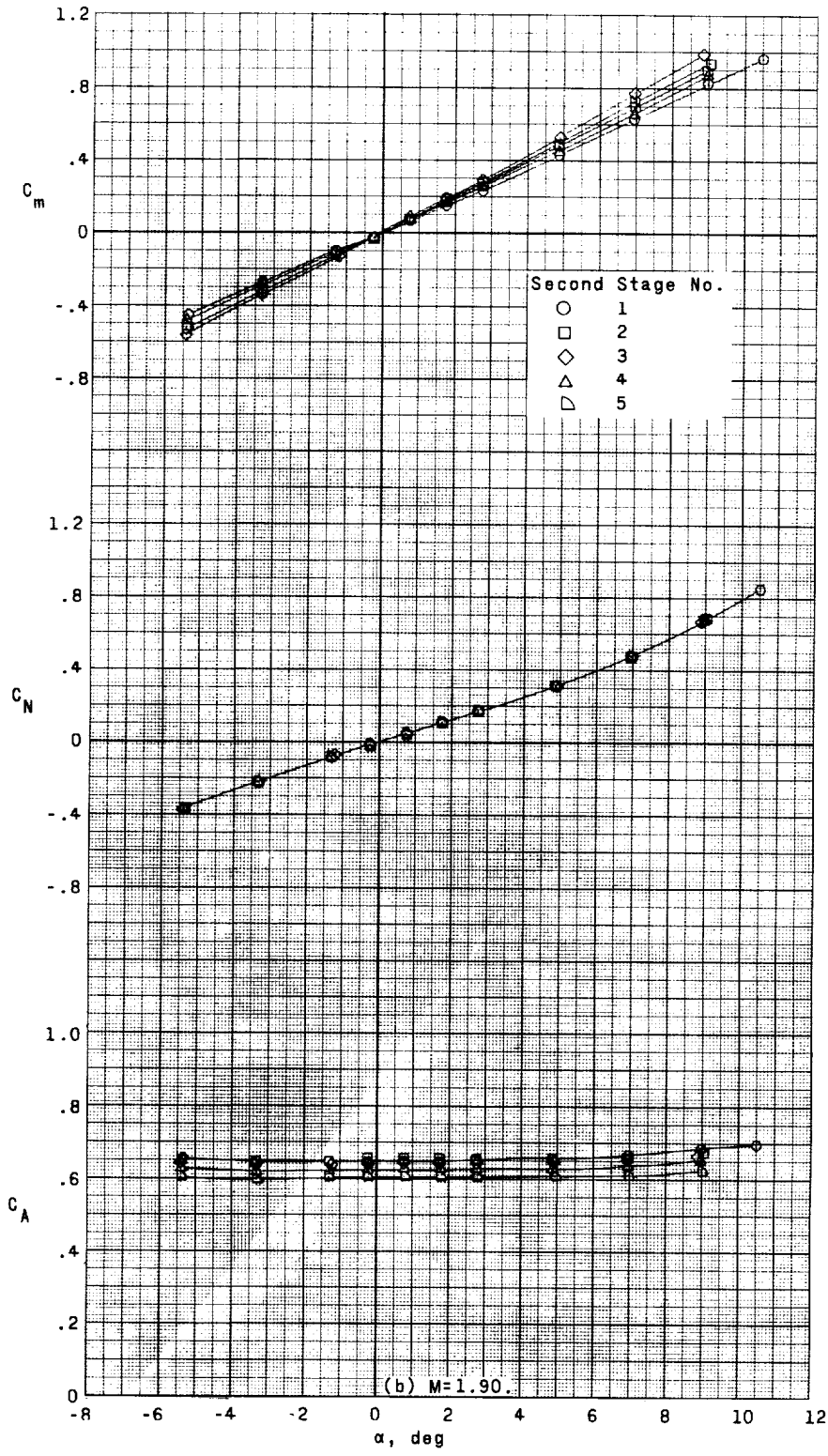

Figure 6.- Continued.

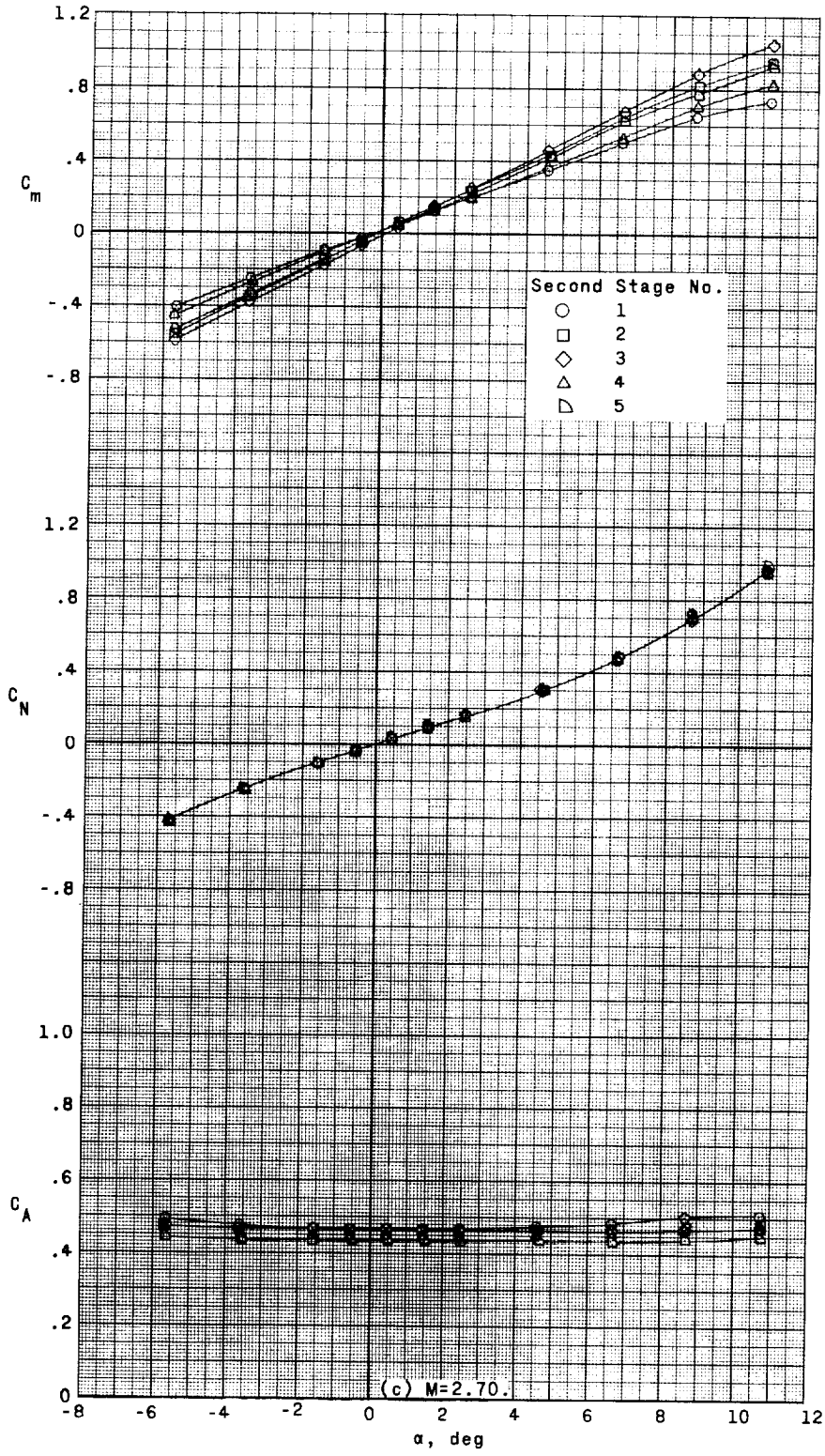

Figure 6.- Continued.

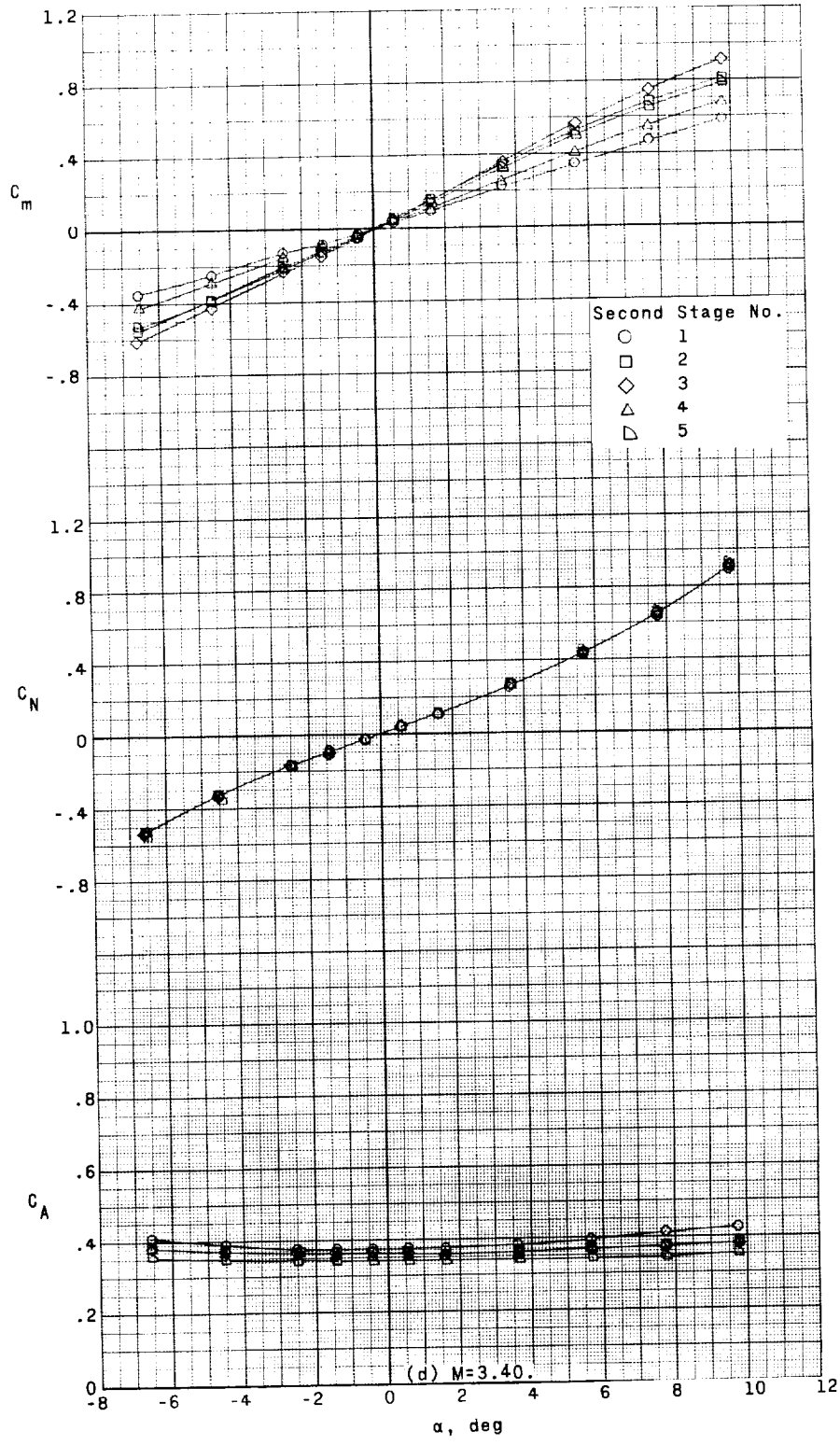

Figure 6.- Concluded.

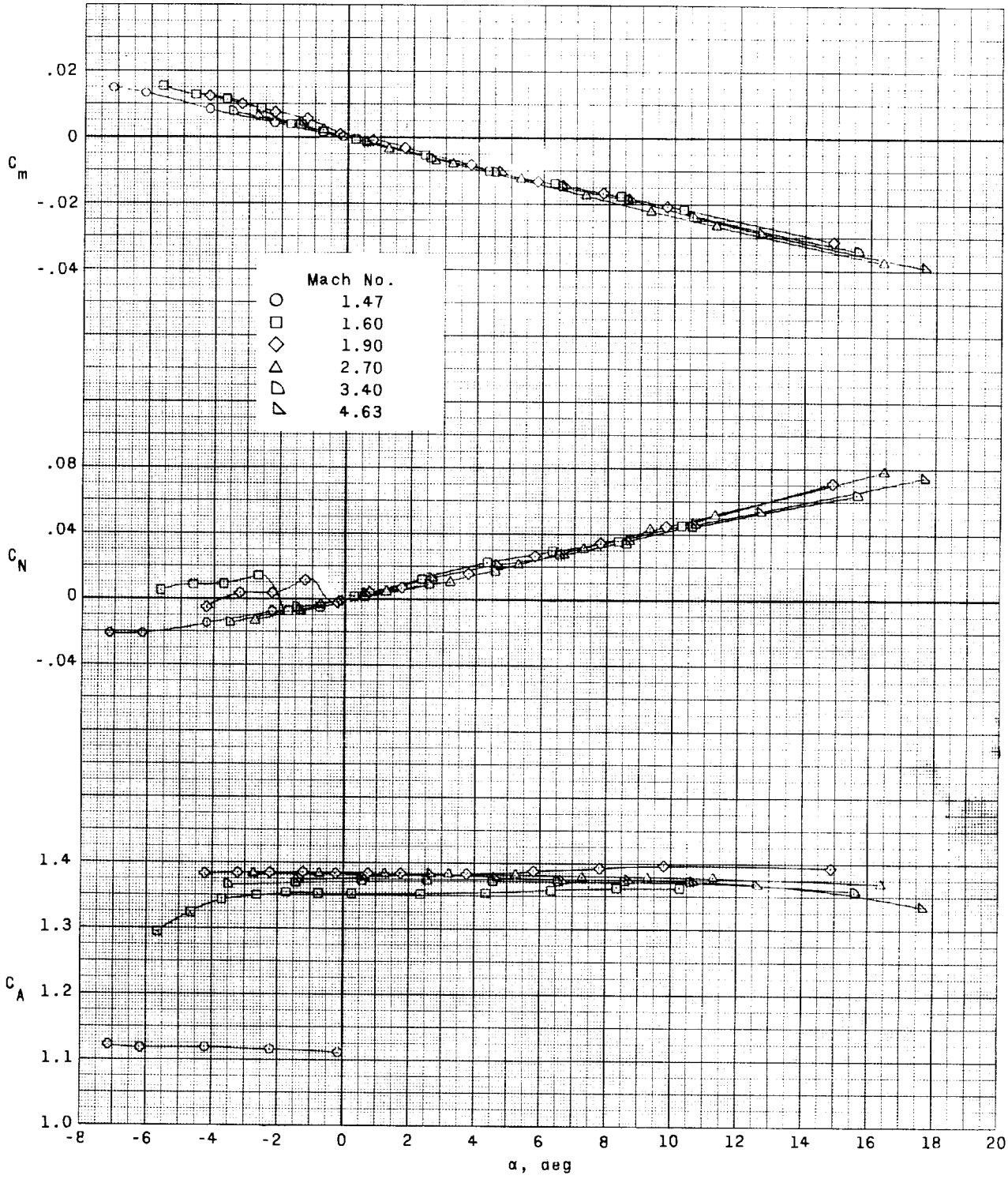

Figure 7.- Aerodynamic characteristics in pitch of the reentry-package configuration.